Supporting Information for

Observation and modelling of OH and HO_2 radicals at a subtropical rural site and implications for secondary pollutants

Zhouxing Zou[1#], Tianshu Chen[1#], Qianjie Chen[1], Weihang Sun[1], Shichun Han[1], Zhuoyue Ren[2], Xinyi Li[2], Wei Song[2], Aoqi Ge[2], Qi Wang[2], Xiao Tian[2], Chenglei Pei[3], Xinming Wang[2], Yanli Zhang[2], and Tao Wang[1]

[#] These authors contributed equally to this work

[1] Department of Civil and Environmental Engineering, The Hong Kong Polytechnic University, Hong Kong, China

[2] Guangzhou Institute of Geochemistry, Chinese Academy of Sciences, Guangzhou, China

[3]Guangdong Province Guangzhou Ecological Environment Monitoring Center Station, Guangzhou 510030, China.

Correspondence to: Tao Wang (tao.wang@polyu.edu.hk)

Contents of this File

14 pages

Figures: S1 to S7

Tables: S1 to S4

Text: S1 to S2

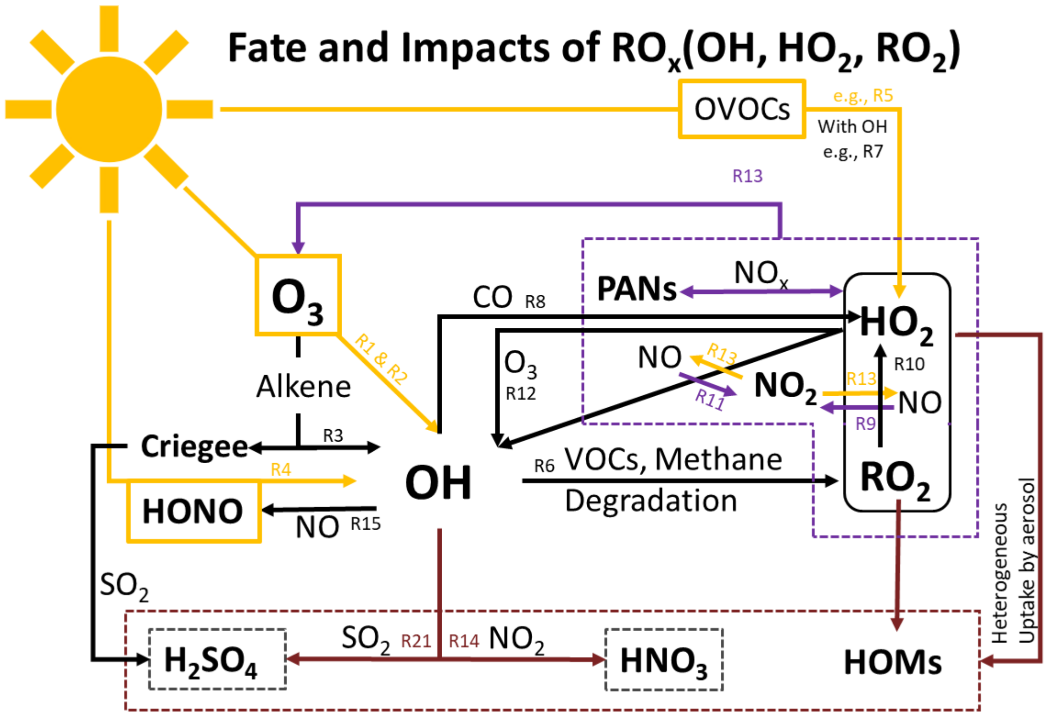

Figure S1 Schematic of the ROx family's photochemical pathway. Photolysis reactions are highlighted in yellow, reactions contributing to secondary aerosol production are marked in brown, and reactions associated with photochemical pollution are indicated in purple. The chemical reactions (R1 to R21) referred to Table S1.

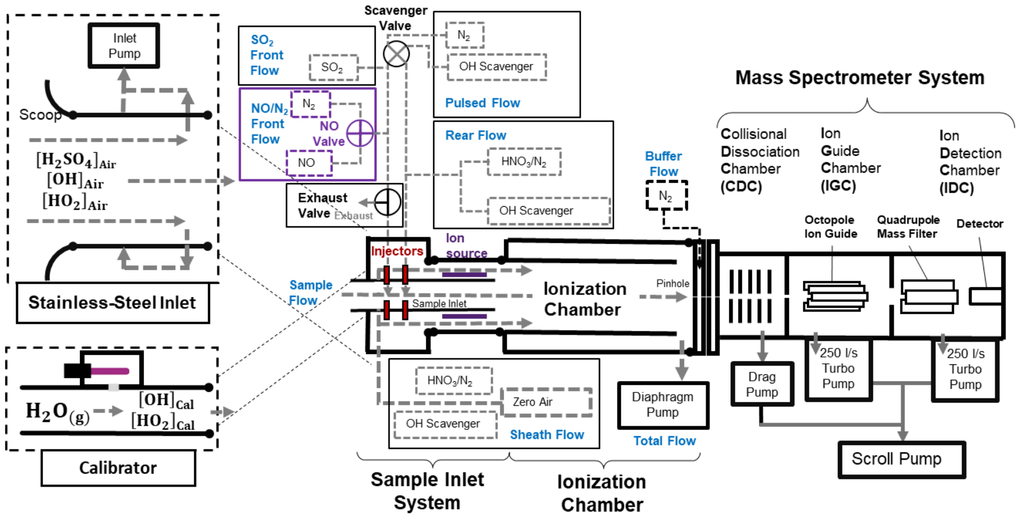

Figure S2 Schematic diagram of the PolyU-CIMS system. The CIMS composed of two detachable components: the stainless-steel inlet and the calibrator; and the main body, which includes the sample inlet system, ionization chamber, and the mass spectrometer system. The frames labeled in purple highlight the additional valve incorporated for HO_2 measurement. Further details on setup, measurement principles of the CIMS are available in a previous study in a previous study (Zou et al., 2023) and Text S1.

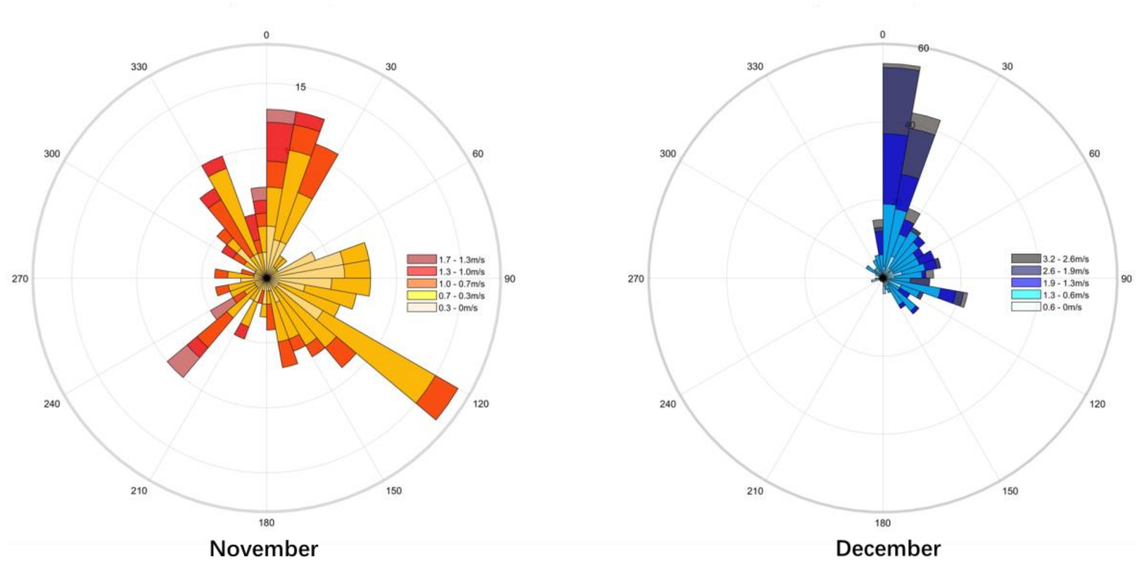

Figure S3 The wind rose for November and December.

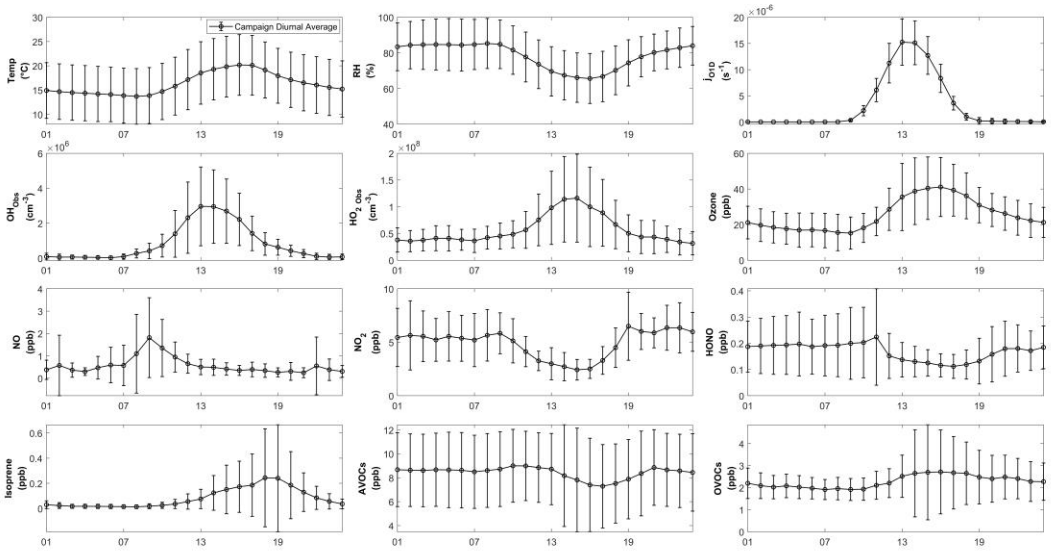

Figure S4 Diurnal profiles of average concentration of HO_2, OH, methodology data and trace gases of the whole campaign. The shade error bars represent standard deviation of the averaged data.

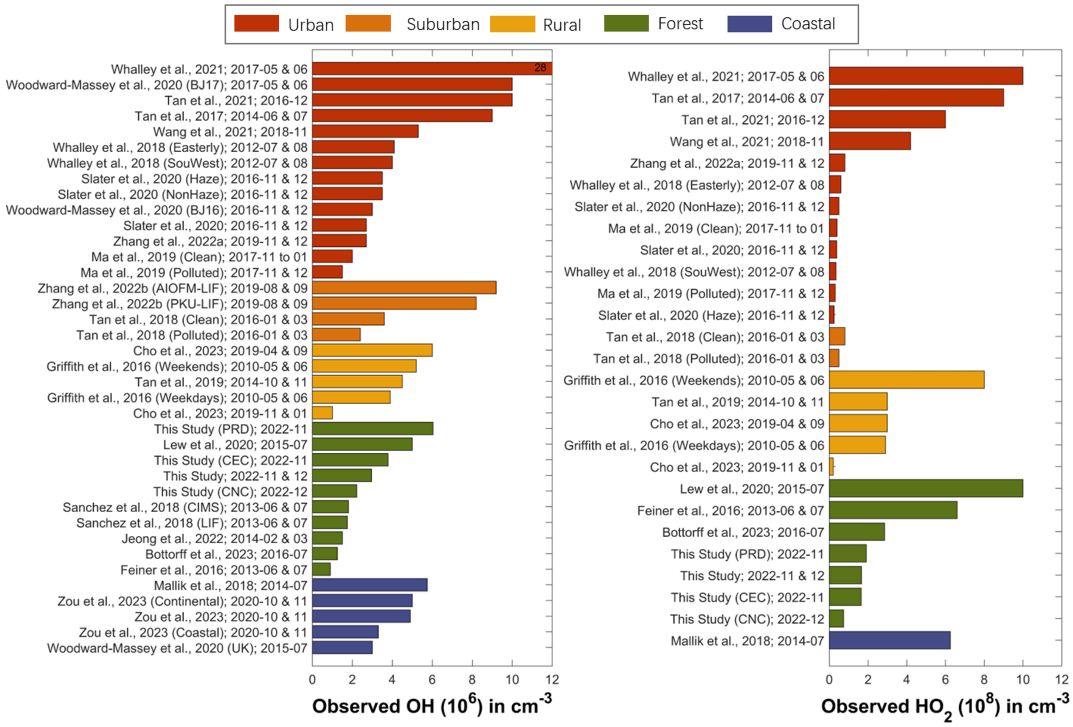

Figure S5 Typical daily averaged maximum concentration of (a) OH and (b) HO_2 observed in various geophysical regions including coastal (blue), forest (green), rural (yellow) and urban (red).

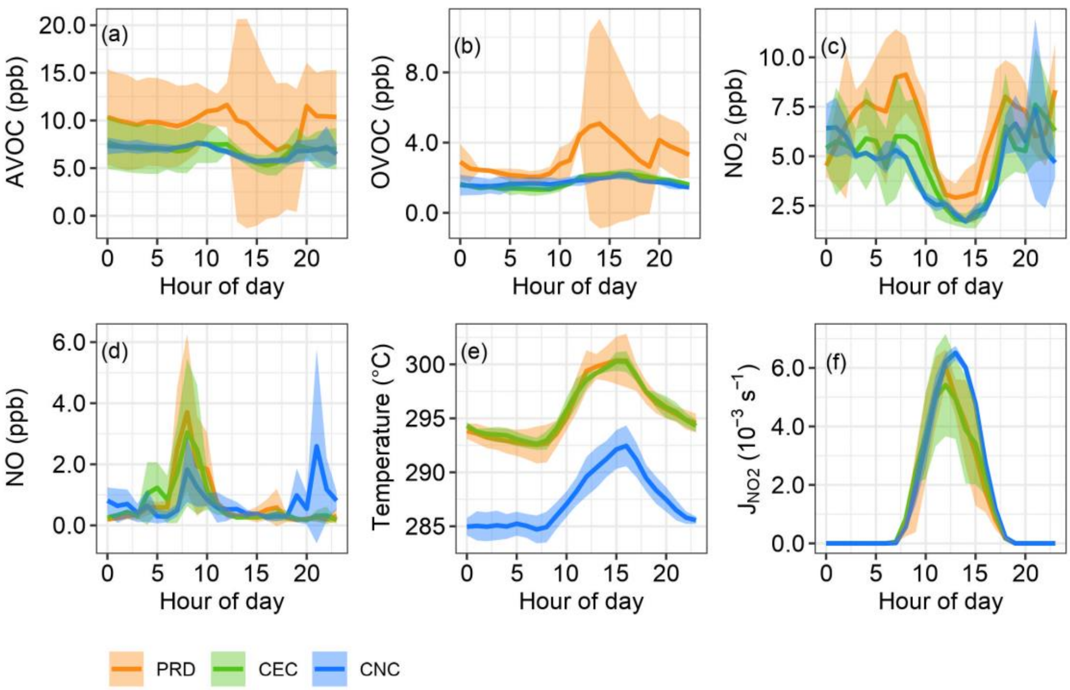

Figure S6 Average diurnal variations of (a) AVOC, (b) OVOC, (c) NO_2, (d) NO, (e) Temperature, and (f) J_{NO2}. The solid-colored lines represent selected cases: orange for PRD, green for CEC, and blue for CNC. The light band represents the standard deviations of the mean.

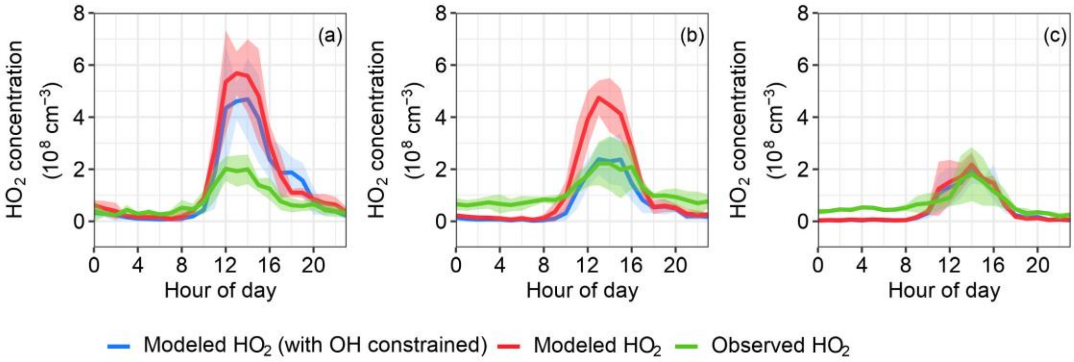

Figure S7 Average diurnal variations of HO_2 for PRD (a), CEC (b), and CNC (c) from observational and modeling results. The solid line represents the average value, while the shaded area indicates one standard deviation. The green line represents the observational results, the red line shows the modeled results without constraining the observed OH concentration (base scenario), and the blue line shows the modeled results with the observed OH concentration constrained.

Table S1 The HO_X related reactions in the model.

Ambient: HO_x Productions	
(R1)	$O_3 + h\nu(<340\ nm) \rightarrow O(^1D) + O_2$
(R2)	$O(^1D) + H_2O \rightarrow OH + OH$
(R3)	$Alkenes + O_3 \rightarrow RO_X + Products$
(R4)	$HONO + h\nu(<400\ nm) \rightarrow OH + NO$
(R5)	$HCHO + h\nu\ (<335\ nm) + 2O_2 \rightarrow 2HO_2 + CO$
Ambient: HO_x Interconvertions	
(R6)	$OH + RH + O_2 \rightarrow RO_2 + H_2O$
(R7)	$HCHO + OH + O_2 \rightarrow CO + H_2O + HO_2$
(R8)	$CO + OH + O_2 \rightarrow CO_2 + HO_2$
(R9)	$RO_2 + NO \rightarrow RO + NO_2$
(R10)	$RO + O_2 \rightarrow R'CHO + HO_2$
(R11)	$HO_2 + NO \rightarrow OH + NO_2$
(R12)	$HO_2 + O_3 \rightarrow OH + 2O_2$
(R13)	$NO_2 + h\nu(<420\ nm) + O_2 \rightarrow NO + O_3$
Ambient: HO_x Loss	
(R14)	$OH + NO_2 \rightarrow HNO_3$
(R15)	$OH + NO \rightarrow HONO$
(R16)	$RO_2 + NO \rightarrow RONO_2$
(R17)	$RO_2 + RO_2 \rightarrow products$
(R18)	$RO_2 + HO_2 \rightarrow ROOH + O_2$
(R19)	$HO_2 + HO_2 \rightarrow H_2O_2 + O_2$
(R20)	$HO_2 + HO_2 + H_2O \rightarrow H_2O_2 + H_2O + O_2$
(R21)	$OH + SO_2 + O_2 + H_2O + M \rightarrow H_2SO_4 + HO_2 + M$
CIMS: Reactions in Sample Inlet System	
(R21)	$OH + SO_2 + O_2 + H_2O + M \rightarrow H_2SO_4 + HO_2 + M$
(R11)	$HO_2 + NO \rightarrow OH + NO_2$
(R22)	$RO_2 + NO + O_2 \rightarrow R'\ CHO + HO_2 + NO_2$
(R23)	$Scavenger\ gas + OH \rightarrow Products$
CIMS: Reactions in Ionization Chamber	
(R24)	$HNO_3 + e^- \rightarrow NO_2^- + OH$
(R25)	$HNO_3 + NO_2^- \rightarrow NO_3^- + HONO$
(R26)	$NO_3^- + (HNO_3)_m + (H_2O)_n + M \rightarrow NO_3^-{\cdot}(HNO_3)_m{\cdot}(H_2O)_n + M$
(R27)	$H_2SO_4 + NO_3^-{\cdot}(HNO_3)_m{\cdot}(H_2O)_n \rightarrow HSO_4^-{\cdot}(HNO_3)_m(H_2O)_n + HNO_3$
CIMS: Reactions in Collisional Dissociation Chamber	
(R28)	$NO_3^-{\cdot}(HNO_3)_m{\cdot}(H_2O)_n + M \rightarrow NO_3^- + (HNO_3)_m + (H_2O)_n + M$
(R29)	$HSO_4^-{\cdot}(HNO_3)_m{\cdot}(H_2O)_n + M \rightarrow HSO_4^- + (HNO_3)_m + (H_2O)_n + M$
CIMS: Calibration	
(R30)	$H_2O + h\nu(184.9nm) + O_2 \rightarrow HO_2 + OH$

Table S2 Overview of instruments used, and species measured during the field campaign.

Instruments	Species	Resolution	Detection Limits	Accuracy
Q-CIMS (NO_3^-)	OH	1 hours	3×10^5 cm^{-3}	± 46%
	HO_2	1 hours	20×10^5 cm^{-3}	± 44%
Thermo 42i-TL	NO	1 min	60 ppt	± 5.2%
Thermo 49i	O_3	1 min	0.5 ppb	± 6.0%
NO_2-11r-EP	NO_2	1 min	60 ppt	± 6.0%
Online GC-MS	VOCs	1 hour	10 ppt	± 20%
Thermo 43i	SO_2	1 min	1 ppb	± 6.1%
Thermo 48i	CO	1 min	40 ppb	± 7.4%
Thermo 17i	NH_3	2 mins	1 ppb	± 8%
SMPS	Aerosol Particles	5 mins	1 particle cm^{-3}	± 10%

Tabel S3 Configurations of the PolyU CIMS in Hok Tsui 2020 and Conghua 2022 campaigns. The changes compare to last configuration were labelled by red color.

a) Hok Tsui 2020

Efficiency Related	Parameters	Gas	Values	Units	Specification for Measurement	Values	Units
E_{Conv}	**Front Injection**	SO_2 (0.9%)	5	sccm	Sample Flow [SO_2]	12	ppm
	Pulse Valve	N_2	2	sccm	Cycle Duration (OH)	6	mins
		C_3F_6 (99.9%)	2	sccm	Scavenging Efficiency (OH)	92%	
	Rear Injection	C_3F_6 (99.9%)	2	sccm	Sample Flow [C_3F_6]	1072	ppm
		HNO_3	10	sccm	Reaction Time	47	ms
	Sample Flow		3.7	slpm	Sample Flow Speed	55	cm/s
E_{Ion}	**Sheath Flow**	Zero Air	12.6	slpm	Reynolds Number in Ionization Chamber	>4000 Turbulent flows	
		HNO_3	10	sccm			
		C_3F_6 (99.9%)	2	sccm	Sheath Flow [C_3F_6]	159	ppm
	Total Flow		16.8	slpm	Sheath Flow Speed	25	cm/s
	Sheath Voltages		-80	V	Voltages Difference for ionization	48	V
	Sample Voltages		-32	V			
E_{Trans}	**Buffer Gas**	N_2	440	sccm	Voltages Difference for transmission	80	V
	Buffer Voltages		-70	V			
	Pinhole Voltages		-40	V			
Cal	**Calibration Flow**		10	slpm	Calibration Factor C_{OH} (Reagent ion: $N^{18}O_3^-$)	1.21×10^{-8}	cm^3
	Flow Speed		65	cm/s			
	Product It Value		8.8×10^{10}	photon/cm			
Uncertainties	**Sigma**			2	**Detection Limit ($\times10^5$ cm^{-3}) (3σ)**	In lab	1.7
	Calibration			38%		Day	12
	Overall			44%		Night	8.5

b) CongHua 2022

Efficiency Related	Parameters	Gas	Values	Units	Specification for Measurement	Values	Units
E_{conv}	**Front Injection**	SO_2 (0.9%)	5	sccm	Sample Flow [SO_2]	12	ppm
		NO (0.9%)	0.5	sccm	Sample Flow [NO]	1.2	ppm
	Pulse Valve	N_2	2	sccm	Cycle Duration (OH)	6	mins
					Cycle Duration (HO_2)	60	mins
		C_3F_6 (99.9%)	2	sccm	Scavenging Efficiency (OH)		90%
					Scavenging Efficiency (HO_2)		60%
	Rear Injection	C_3F_6 (99.9%)	2	sccm	Sample Flow [C_3F_6]	1072	ppm
		HNO_3	10	sccm	Reaction Time	47	ms
	Sample Flow		3.7	slpm	Sample Flow Speed	55	cm/s
E_{Ion}	**Sheath Flow**	Zero Air	12.6	slpm	Reynolds Number in Ionization Chamber	>4000 Turbulent flows	
		HNO_3	10	sccm			
		C_3F_6 (99.9%)	2	sccm	Sheath Flow [C_3F_6]	159	ppm
	Total Flow		16.8	slpm	Sheath Flow Speed	25	cm/s
	Sheath Voltages		-80	V	Voltages Difference for ionization	48	V
	Sample Voltages		-32	V			
E_{Trans}	**Buffer Gas**	N_2	440	sccm	Voltages Difference for transmission	80	V
	Buffer Voltages		-70	V			
	Pinhole Voltages		-40	V			
Cal	**Calibration Flow**		10	slpm	Calibration Factors ($N^{18}O_3^-$) C_{OH}	1.09×10^{-8}	cm^3
	Flow Speed		65	cm/s	C_{HO2}	1.07×10^{-8}	
	Product It Value		8.8×10^{10}	photon/cm	C_{H2SO4}	6.01×10^{-9}	
Overall Uncertainties (2σ)		OH		46%	**Detection Limit in Field Study ($\times10^5$ cm^{-3}) (3σ)**	OH	3
		H_2SO_4		40%		H_2SO_4	1
		HO_2		44%		HO_2	20

Table S4 Average concentrations and standard deviation of measured VOCs that are constrained in the box model in the entire campaign and in different cases.

Species	Total	PRD	CEC	CNC	MCM Abb.
Ethane	2.3±0.83	2.2±1.2	2.4±0.89	2.3±0.62	C2H6
Ethylene	0.69±0.33	0.72±0.32	0.85±0.47	0.59±0.23	C2H4
Propane	1.6±0.62	2.2±0.71	1.6±0.61	1.4±0.46	C3H8
Propene	0.072±0.077	0.11±0.15	0.074±0.051	0.055±0.032	C3H6
i-Butane	0.44±0.28	0.8±0.46	0.45±0.15	0.31±0.094	IC4H10
n-Butane	0.65±0.41	1.2±0.65	0.64±0.25	0.48±0.16	NC4H10
Acetylene	0.92±0.42	1.1±0.46	1.1±0.46	0.78±0.35	C2H2
trans-2-Butene	0.015±0.0071	0.015±0.0057	0.018±0.01	0.014±0.0057	TBUT2ENE
cis-2-Butene	0.083±0.038	0.14±0.047	0.08±0.013	0.066±0.017	CBUT2ENE
Butene	0.044±0.021	0.044±0.044	0.043±0.015	0.044±0.0098	BUT1ENE
Chloromethane	0.84±0.22	0.66±0.28	0.88±0.15	0.86±0.2	CH3CL
1,3-Butadiene	0.0079±0.0078	0.011±0.0087	0.011±0.012	0.0051±0.0036	C4H6
Acetaldehyde	0.92±0.35	1.5±0.37	NaN	0.82±0.27	CH3CHO
Bromomethane	0.0093±0.0022	0.011±0.0022	0.01±0.0022	0.0083±0.0018	CH3BR
Chloroethane	0.023±0.012	0.022±0.016	0.026±0.011	0.021±0.011	CH3CH2CL
i-Pentane	0.34±0.17	0.57±0.21	0.39±0.11	0.24±0.061	IC5H12
1-Pentene	0.043±0.016	0.062±0.023	0.042±0.014	0.037±0.0081	PENT1ENE
n-Pentane	0.19±0.1	0.3±0.17	0.17±0.069	0.15±0.049	NC5H12
trans-2-Pentene	0.0032±0.0045	0.0098±0.0055	0.0041±0.0038	0.0083±0.0076	TPENT2ENE
Isoprene	0.082±0.17	0.22±0.3	0.14±0.17	0.016±0.019	C5H8
cis-2-Pentene	0.0017±0.0028	0.0061±0.0032	0.0022±0.002	0.0023±0.0044	CPENT2ENE
Acrolein	0.06±0.031	0.095±0.04	0.065±0.029	0.05±0.019	ACR
Propanal	0.011±0.0059	0.015±0.0099	0.011±0.0044	0.011±0.0039	C2H5CHO
Vinylidene chloride	0.0036±0.0027	0.0031±0.0015	0.0025±0.0019	0.0035±0.0022	CCL2CH2
2,2-Dimethylbutane	0.017±0.015	0.039±0.025	0.017±0.0064	0.0098±0.0018	M22C4
Dichloromethane	1.1±0.84	2.2±1.3	1.2±0.37	0.75±0.33	CH2CL2
2,3-Dimethylbutane	0.026±0.023	0.058±0.031	0.033±0.017	0.014±0.0045	M23C4
2-Methylpentane	0.071±0.045	0.16±0.083	0.081±0.032	0.052±0.015	M2PE
3-Methylpentane	0.052±0.039	0.1±0.059	0.055±0.022	0.032±0.012	M3PE
Methyl tert-butyl ether	0.072±0.042	0.13±0.048	0.09±0.032	0.045±0.018	MTBE
1-Hexene	0.0048±0.0052	0.013±0.0036	0.0067±0.0055	0.0016±0.00095	HEX1ENE
n-Hexane	0.066±0.043	0.12±0.057	0.07±0.033	0.044±0.022	NC6H14
Methacrolein	0.062±0.062	0.13±0.058	0.11±0.063	0.022±0.0091	MACR
1,1-Dichloroethane	0.0086±0.0046	0.011±0.0057	0.011±0.005	0.0068±0.0037	CHCL2CH3
Butyraldehyde	0.54±0.21	0.46±0.17	0.48±0.15	0.57±0.23	C3H7CHO
1,2-Dichloroethylene	0.049±0.076	0.12±0.15	0.046±0.033	0.03±0.02	DICLETH
2-Butanone	0.25±0.24	0.53±0.43	0.27±0.12	0.16±0.077	MEK
Ethyl acetate	0.27±0.39	0.62±0.77	0.24±0.17	0.17±0.11	ETHACET
Chloroform	0.082±0.032	0.12±0.038	0.096±0.018	0.064±0.021	CHCL3
Methylchloroform	0.0021±0.0011	0.0037±0.00045	0.0019±0.0013	0.0016±0.00047	CH3CCL3
2-Methylhexane	0.015±0.017	0.039±0.027	0.015±0.0075	0.0074±0.0027	M2HEX
Cyclohexane	0.019±0.015	0.038±0.019	0.021±0.015	0.011±0.0058	CHEX
Tetrachloromethane	0.073±0.0055	0.072±0.0048	0.07±0.0062	0.075±0.005	CCL4
3-Methylhexane	0.02±0.024	0.054±0.041	0.019±0.01	0.0087±0.0033	M3HEX
Benzene	0.35±0.14	0.36±0.15	0.4±0.15	0.31±0.13	BENZENE
Ethylene dichloride	0.36±0.17	0.33±0.17	0.4±0.19	0.33±0.17	CH2CLCH2CL
n-Hepane	0.035±0.023	0.067±0.034	0.034±0.013	0.025±0.0064	NC7H16
Crotonaldehyde	0.45±0.14	0.47±0.0088	0.48±0.0064	0.39±0.21	C3MDBAL
Trichloroethene	0.021±0.023	0.051±0.036	0.024±0.017	0.01±0.0039	TRICLETH
1,2-Dichloropropane	0.085±0.038	0.12±0.028	0.11±0.026	0.062±0.031	CL12PROP
Pantanal	0.018±0.011	0.033±0.017	0.02±0.0075	0.014±0.005	C4H9CHO
1,3-Dichloro-1-propene	0.0025±0.0011	0.0031±0.00081	0.0023±0.0014	0.0024±0.0011	CLC3H4CL
4-Methyl-2-pentanone	0.0046±0.0073	0.017±0.0046	0.0055±0.006	0.0027±0.0047	MIBK
Toluene	0.28±0.27	0.61±0.46	0.29±0.12	0.17±0.075	TOLUENE
n-Octane	0.0093±0.0071	0.021±0.0063	0.0093±0.0065	0.0056±0.0018	NC8H18
1,1,2-Trichloroethane	0.014±0.0097	0.015±0.01	0.019±0.013	0.011±0.006	CH2CLCHCL2
Tetrachloroethylene	0.015±0.013	0.036±0.017	0.016±0.0045	0.0076±0.0029	TCE
2-Hexanone	0.05±0.025	0.086±0.026	0.06±0.011	0.038±0.011	HEX2ONE
Hexanal	0.041±0.022	0.074±0.023	0.05±0.0094	0.03±0.0086	C5H11CHO
1,2-Dibromoethane	0.002±0.0016	0.0039±0.0013	0.0021±0.0016	0.0014±0.0011	DIBRET
Ethylbenzene	0.042±0.031	0.066±0.032	0.044±0.033	0.031±0.025	EBENZ
o-Xylene	0.039±0.03	0.071±0.037	0.043±0.029	0.027±0.019	OXYL
Styrene	0.02±0.013	0.032±0.0087	0.017±0.0096	0.01±0.007	STYRENE
Isopropylbenzene	0.006±0.0058	0.016±0.0026	0.0068±0.0058	0.0026±0.0012	IPBENZ
1,1,2,2-Tetrachloroethane	0.0031±0.0019	0.0053±0.0012	0.0037±0.0019	0.0022±0.0012	CHCL2CHCL2
n-Propylbenzene	0.0048±0.0045	0.012±0.0032	0.0058±0.0039	0.0021±0.0013	PBENZ
m-Ethyltoluene	0.0073±0.0067	0.017±0.0079	0.0087±0.0047	0.0036±0.0022	METHTOL
p-Ethyltoluene	0.0048±0.0047	0.012±0.0044	0.0056±0.0038	0.0023±0.0017	PETHTOL
1,3,5-Trimethylbenzene	0.0051±0.0054	0.014±0.0052	0.0063±0.0037	0.002±0.0016	TM135B
n-Decane	0.0031±0.0031	0.0083±0.0026	0.0034±0.0024	0.0014±0.00056	NC10H22
Benzaldehyde	0.0047±0.0044	0.012±0.0038	0.0055±0.0034	0.0021±0.0011	BENZAL
1,2,4-Trimethylbenzene	0.0088±0.009	0.022±0.012	0.011±0.0049	0.0041±0.0022	TM124B
1,2,3-Trimethylbenzene	0.0037±0.0035	0.0093±0.0036	0.0043±0.0023	0.0017±0.001	TM123B
Undecane	0.0019±0.0024	0.0058±0.0012	0.0029±0.0017	0.0034±0.0051	NC11H24
Dodecane	0.0094±0.0035	0.014±0.0034	0.008±0.0022	0.008±0.0024	NC12H26

Text S1 Modification for HO_2 measurement

To measure the HO_2, a valve was added to switch the injection gas between NO and N_2 gases as indicated by purple frame in Figure S2. When NO is added to the sample flow, the CIMS switches to HO_2 mode for total HO_x measurement, whereas adding N_2 shifts it to OH mode for OH measurement. It should be noted that the increasing NO concentration can enhance HO_2 conversion (R11), but excessive NO levels trigger the HONO formation (R15), competing with the conversion process (R21) and lowering the detection efficiency. Consequently, the NO to SO_2 concentration ratio is crucial for HO_2 measurements. Sensitivity tests revealed an optimal [NO]/[SO2] ratio of 0.1 for the PolyU-CIMS, aligning with prior research recommendations (Edwards et al., 2003; Sjostedt et al., 2007).

Text S2 Measurement interferences

The concentration of injected NO is the primary source of HO_2 measurement interference in this study. High NO concentrations convert ambient RO_2, particularly alkene and aromatic-related RO_2, into HO_2 and then OH, leading to a positive bias in HO_2 measurements (Fuchs et al., 2014). To mitigate this interference, the NO concentration at the sample inlet was set to 1.2 ppm—lower than the levels recommended in previous studies to minimize RO_2 interference (Fuchs et al., 2014). Additionally, a box model was employed to quantify and subtract this interference from the observational results.

The OH interference in PolyU-CIMS, resulting from ambient HO_2 recycling (R11) and ionization process (R24, artificial OH), was accounted for and included in the measurement uncertainty, as outlined by Zou et al. (2023). However, in this study, PolyU-CIMS encountered additional interference from residual NO in the injectors when switching from NO (used for HO_2 measurement) to N_2 (used for OH measurement). To prevent residual NO buildup, the inlet was cleaned daily, and a one-hour calibration was performed at both the start and end of daily measurement to monitor the NO residuals. The monitoring results showed that the NO residual time for PolyU - CIMS was approximately 26 mins which is similar to the residual time reported in earlier studies (Edwards et al., 2003; Sjostedt et al., 2007). Consequently, data collected during the residual period (30 mins after switching the measurement target from HO_2 to OH) were discarded to eliminate any NO residual interference from the final results.

Reference

Bottorff, B., Lew, M. M., Woo, Y., Rickly, P., Rollings, M. D., Deming, B., Anderson, D. C., Wood, E., Alwe, H. D., Millet, D. B., Weinheimer, A., Tyndall, G., Ortega, J., Dusanter, S., Leonardis, T., Flynn, J., Erickson, M., Alvarez, S., Rivera-Rios, J. C., Shutter, J. D., Keutsch, F., Helmig, D., Wang, W., Allen, H. M., Slade, J. H., Shepson, P. B., Bertman, S., and Stevens, P. S.: OH, HO_2, and RO_2 radical chemistry in a rural forest environment: measurements, model comparisons, and evidence of a missing radical sink, Atmospheric Chemistry and Physics, 23, 10287–10311, https://doi.org/10.5194/acp-23-10287-2023, 2023.

Cho, C., Fuchs, H., Hofzumahaus, A., Holland, F., Bloss, W. J., Bohn, B., Dorn, H.-P., Glowania, M., Hohaus, T., Liu, L., Monks, P. S., Niether, D., Rohrer, F., Sommariva, R., Tan, Z., Tillmann, R., Kiendler-Scharr, A., Wahner, A., and Novelli, A.: Experimental chemical budgets of OH, HO_2, and RO_2 radicals in rural air in western Germany during the JULIAC campaign 2019, Atmospheric Chemistry and Physics, 23, 2003–2033, https://doi.org/10.5194/acp-23-2003-2023, 2023.

Edwards, G. D., Cantrell, C. A., Stephens, S., Hill, B., Goyea, O., Shetter, R. E., Mauldin, R. L., Kosciuch, E., Tanner, D. J., and Eisele, F. L.: Chemical Ionization Mass Spectrometer Instrument for the Measurement of Tropospheric HO_2 and RO_2, Anal. Chem., 75, 5317–5327, https://doi.org/10.1021/ac034402b, 2003.

Feiner, P. A., Brune, W. H., Miller, D. O., Zhang, L., Cohen, R. C., Romer, P. S., Goldstein, A. H., Keutsch, F. N., Skog, K. M., Wennberg, P. O., Nguyen, T. B., Teng, A. P., DeGouw, J., Koss, A., Wild, R. J., Brown, S. S., Guenther, A., Edgerton, E., Baumann, K., and Fry, J. L.: Testing Atmospheric Oxidation in an Alabama Forest, Journal of the Atmospheric Sciences, 73, 4699–4710, https://doi.org/10.1175/JAS-D-16-0044.1, 2016.

Fuchs, H., Acir, I.-H., Bohn, B., Brauers, T., Dorn, H.-P., Häseler, R., Hofzumahaus, A., Holland, F., Kaminski, M., Li, X., Lu, K., Lutz, A., Nehr, S., Rohrer, F., Tillmann, R., Wegener, R., and Wahner, A.: OH regeneration from methacrolein oxidation investigated in the atmosphere simulation chamber SAPHIR, Atmos. Chem. Phys., 14, 7895–7908, https://doi.org/10.5194/acp-14-7895-2014, 2014.

Griffith, S. M., Hansen, R. F., Dusanter, S., Michoud, V., Gilman, J. B., Kuster, W. C., Veres, P. R., Graus, M., Gouw, J. A., Roberts, J., Young, C., Washenfelder, R., Brown, S. S., Thalman, R., Waxman, E., Volkamer, R., Tsai, C., Stutz, J., Flynn, J. H., Grossberg, N., Lefer, B., Alvarez, S. L., Rappenglueck, B., Mielke, L. H., Osthoff, H. D., and

Stevens, P. S.: Measurements of hydroxyl and hydroperoxy radicals during CalNex-LA: Model comparisons and radical budgets, J. Geophys. Res. Atmos., 121, 4211–4232, https://doi.org/10.1002/2015JD024358, 2016.

Jeong, D., Seco, R., Emmons, L., Schwantes, R., Liu, Y., McKinney, K. A., Martin, S. T., Keutsch, F. N., Gu, D., Guenther, A. B., Vega, O., Tota, J., Souza, R. A. F., Springston, S. R., Watson, T. B., and Kim, S.: Reconciling Observed and Predicted Tropical Rainforest OH Concentrations, JGR Atmospheres, 127, https://doi.org/10.1029/2020JD032901, 2022.

Lew, M. M., Rickly, P. S., Bottorff, B. P., Reidy, E., Sklaveniti, S., Léonardis, T., Locoge, N., Dusanter, S., Kundu, S., Wood, E., and Stevens, P. S.: OH and HO_2 radical chemistry in a midlatitude forest: measurements and model comparisons, Atmospheric Chemistry and Physics, 20, 9209–9230, https://doi.org/10.5194/acp-20-9209-2020, 2020.

Ma, X., Tan, Z., Lu, K., Yang, X., Liu, Y., Li, S., Li, X., Chen, S., Novelli, A., Cho, C., Zeng, L., Wahner, A., and Zhang, Y.: Winter photochemistry in Beijing: Observation and model simulation of OH and HO2 radicals at an urban site, Science of The Total Environment, 685, 85–95, https://doi.org/10.1016/j.scitotenv.2019.05.329, 2019.

Mallik, C., Tomsche, L., Bourtsoukidis, E., Crowley, J. N., Derstroff, B., Fischer, H., Hafermann, S., Hüser, I., Javed, U., Keßel, S., Lelieveld, J., Martinez, M., Meusel, H., Novelli, A., Phillips, G. J., Pozzer, A., Reiffs, A., Sander, R., Taraborrelli, D., Sauvage, C., Schuladen, J., Su, H., Williams, J., and Harder, H.: Oxidation processes in the eastern Mediterranean atmosphere: evidence from the modelling of HO_x measurements over Cyprus, Atmospheric Chemistry and Physics, 18, 10825–10847, https://doi.org/10.5194/acp-18-10825-2018, 2018.

Sanchez, D., Jeong, D., Seco, R., Wrangham, I., Park, J.-H., Brune, W. H., Koss, A., Gilman, J., de Gouw, J., Misztal, P., Goldstein, A., Baumann, K., Wennberg, P. O., Keutsch, F. N., Guenther, A., and Kim, S.: Intercomparison of OH and OH reactivity measurements in a high isoprene and low NO environment during the Southern Oxidant and Aerosol Study (SOAS), Atmospheric Environment, 174, 227–236, https://doi.org/10.1016/j.atmosenv.2017.10.056, 2018.

Sjostedt, S. J., Huey, L. G., Tanner, D. J., Peischl, J., Chen, G., Dibb, J. E., Lefer, B., Hutterli, M. A., Beyersdorf, A. J., Blake, N. J., Blake, D. R., Sueper, D., Ryerson, T., Burkhart, J., and Stohl, A.: Observations of hydroxyl and the sum of peroxy radicals at Summit, Greenland during summer 2003, Atmospheric Environment, 41, 5122–5137, https://doi.org/10.1016/j.atmosenv.2006.06.065, 2007.

Slater, E. J., Whalley, L. K., Woodward-Massey, R., Ye, C., Lee, J. D., Squires, F., Hopkins, J. R., Dunmore, R. E., Shaw, M., Hamilton, J. F., Lewis, A. C., Crilley, L. R., Kramer, L., Bloss, W., Vu, T., Sun, Y., Xu, W., Yue, S., Ren, L., Acton, W. J. F., Hewitt, C. N., Wang, X., Fu, P., and Heard, D. E.: Elevated levels of OH observed in haze events during wintertime in central Beijing, Atmospheric Chemistry and Physics, 20, 14847–14871, https://doi.org/10.5194/acp-20-14847-2020, 2020.

Tan, Z., Fuchs, H., Lu, K., Hofzumahaus, A., Bohn, B., Broch, S., Dong, H., Gomm, S., Häseler, R., He, L., Holland, F., Li, X., Liu, Y., Lu, S., Rohrer, F., Shao, M., Wang, B., Wang, M., Wu, Y., Zeng, L., Zhang, Y., Wahner, A., and Zhang, Y.: Radical chemistry at a rural site (Wangdu) in the North China Plain: observation and model calculations of OH, HO_2 and RO_2 radicals, Atmospheric Chemistry and Physics, 17, 663–690, https://doi.org/10.5194/acp-17-663-2017, 2017.

Tan, Z., Rohrer, F., Lu, K., Ma, X., Bohn, B., Broch, S., Dong, H., Fuchs, H., Gkatzelis, G. I., Hofzumahaus, A., Holland, F., Li, X., Liu, Y., Liu, Y., Novelli, A., Shao, M., Wang, H., Wu, Y., Zeng, L., Hu, M., Kiendler-Scharr, A., Wahner, A., and Zhang, Y.: Wintertime photochemistry in Beijing: observations of RO_x radical concentrations in the North China Plain during the BEST-ONE campaign, Atmospheric Chemistry and Physics, 18, 12391–12411, https://doi.org/10.5194/acp-18-12391-2018, 2018.

Tan, Z., Lu, K., Jiang, M., Su, R., Wang, H., Lou, S., Fu, Q., Zhai, C., Tan, Q., Yue, D., Chen, D., Wang, Z., Xie, S., Zeng, L., and Zhang, Y.: Daytime atmospheric oxidation capacity in four Chinese megacities during the photochemically polluted season: a case study based on box model simulation, Atmos. Chem. Phys., 19, 3493–3513, https://doi.org/10.5194/acp-19-3493-2019, 2019.

Tan, Z., Ma, X., Lu, K., Jiang, M., Zou, Q., Wang, H., Zeng, L., and Zhang, Y.: Direct evidence of local photochemical production driven ozone episode in Beijing: A case study, Science of The Total Environment, 800, 148868, https://doi.org/10.1016/j.scitotenv.2021.148868, 2021.

Wang, G., Iradukunda, Y., Shi, G., Sanga, P., Niu, X., and Wu, Z.: Hydroxyl, hydroperoxyl free radicals determination methods in atmosphere and troposphere, Journal of Environmental Sciences, 99, 324–335, https://doi.org/10.1016/j.jes.2020.06.038, 2021.

Whalley, L. K., Stone, D., Dunmore, R., Hamilton, J., Hopkins, J. R., Lee, J. D., Lewis, A. C., Williams, P., Kleffmann, J., Laufs, S., Woodward-Massey, R., and Heard, D. E.: Understanding in situ ozone production in the summertime through radical observations and modelling studies during the Clean air for London project (ClearfLo), Atmos. Chem. Phys., 18, 2547–2571, https://doi.org/10.5194/acp-18-2547-2018, 2018.

Whalley, L. K., Slater, E. J., Woodward-Massey, R., Ye, C., Lee, J. D., Squires, F., Hopkins, J. R., Dunmore, R. E., Shaw, M., Hamilton, J. F., Lewis, A. C., Mehra, A., Worrall, S. D., Bacak, A., Bannan, T. J., Coe, H., Percival, C. J., Ouyang, B., Jones, R. L., Crilley, L. R., Kramer, L. J., Bloss, W. J., Vu, T., Kotthaus, S., Grimmond, S., Sun, Y., Xu, W., Yue, S., Ren, L., Acton, W. J. F., Hewitt, C. N., Wang, X., Fu, P., and Heard, D. E.: Evaluating the sensitivity of radical chemistry and ozone formation to ambient VOCs and NO_x in Beijing, Atmospheric Chemistry and Physics, 21, 2125–2147, https://doi.org/10.5194/acp-21-2125-2021, 2021.

Woodward-Massey, R., Slater, E. J., Alen, J., Ingham, T., Cryer, D. R., Stimpson, L. M., Ye, C., Seakins, P. W., Whalley, L. K., and Heard, D. E.: Implementation of a chemical background method for atmospheric OH measurements by laser-induced fluorescence:

characterisation and observations from the UK and China, Atmospheric Measurement Techniques, 13, 3119–3146, https://doi.org/10.5194/amt-13-3119-2020, 2020.

Zhang, G., Hu, R., Xie, P., Lu, K., Lou, S., Liu, X., Li, X., Wang, F., Wang, Y., Yang, X., Cai, H., Wang, Y., and Liu, W.: Intercomparison of OH radical measurement in a complex atmosphere in Chengdu, China, Science of The Total Environment, 838, 155924, https://doi.org/10.1016/j.scitotenv.2022.155924, 2022a.

Zhang, G., Hu, R., Xie, P., Lou, S., Wang, F., Wang, Y., Qin, M., Li, X., Liu, X., Wang, Y., and Liu, W.: Observation and simulation of HO_x radicals in an urban area in Shanghai, China, Science of The Total Environment, 810, 152275, https://doi.org/10.1016/j.scitotenv.2021.152275, 2022b.

Zou, Z., Chen, Q., Xia, M., Yuan, Q., Chen, Y., Wang, Y., Xiong, E., Wang, Z., and Wang, T.: OH measurements in the coastal atmosphere of South China: possible missing OH sinks in aged air masses, Atmospheric Chemistry and Physics, 23, 7057–7074, https://doi.org/10.5194/acp-23-7057-2023, 2023.